Article

Advantages and Limitations to the Use of Optical Measurements to Study Sediment Dynamics.

Emmanuel Boss [1]*, **Christopher R. Sherwood** [2], **Paul Hill** [3] **and Tim Milligan** [3]

[1]   University of Maine; emmanuel.boss@maine.edu
[2]   U.S. Geological Survey, Woods Hole, MA 02543 U.S.A.; csherwood@usgs.gov
[3]   Dalhousie University; paul.hill@dal.ca
*   Correspondence: emmanuel.boss@maine.edu; Tel.: +1-207-745-3061
†   University of Maine, School of Marine Sciences, 5706 Aubert Hall, Orono, ME 04473, USA

Abstract: Measurements of optical properties have been used for decades to study particle distributions in the ocean. They have been found useful to constrain suspended mass concentration as well as particle-related properties such as size, composition, packing (particle porosity or density) and settling velocity. Optical properties, however, provide measurements that are biased, as certain particles (based on size, composition, shape or packing) contribute to a specific property more than others. Here we study this issue both theoretically as well as by contrasting different optical properties collected simultaneously in a bottom boundary layer, to highlight the utility of such measurements as well as the biases we are likely to encounter using different optical properties to study suspended particles. In particular, we investigate the possibility to infer settling velocity from vertical profiles of optical measurements, finding that the effects of aggregation dynamics can seldom be ignored.
NB: This draft manuscript is distributed solely for purposes of scientific peer review. Its content is deliberative and pre-decisional, so it must not be disclosed or released by reviewers. Because the manuscript has not yet been approved for publication by the U.S. Geological Survey (USGS), it does not represent any official USGS finding or policy.

Data Set License: The data presented in this paper are in the public domain in the United States because they come from the United States Geological Survey, an agency of the United States Department of Interior.

---

1. Introduction

Optical properties have long been used to study suspended particles and their dynamics (e.g. reviews by [1–3]). The most commonly measured optical properties are attenuation and scattering at different angles (both forward and back). Other optical devices, including ambient radiation sensors, cameras, and holographic instruments also produce valuable data, but this paper will focus primarily on measurements of attenuation and scattering. Measurement volumes are typically small (from a few ml to tens of ml) and temporal averaging can increase the likelihood that rare large particles are sampled. Optical measurements can provide relatively direct estimates of mass or volume concentrations and particle size, and can also be used to infer information about particle

density, composition, and settling velocity. The primary advantages of using optical properties to study suspended particles are that they can be obtained at high frequency over long periods, and they are relatively non-invasive. Optical measurements are affected by all the particles in the suspension sampled, but as we explain below, they do not respond to all particles equally.

Some known disadvantages of optical instrument are (1) they saturate at high SPM loads (e.g. [2]), (2) even though small they are intrusive (producing a turbulent wake when in current), (3) they can be affected by ambient light, (4) they can be power hungry, and (5) they are susceptible to bio-fouling.

1.1. Optical proxies of properties of sediment particles

Volume and Mass Concentration The O(1) variation in optical signals measured in the field is due to changes in suspended particle mass concentrations (SPM; e.g. [5]). SPM is typically estimated with optical properties measured at red wavelengths (e.g. 660nm), minimizing the impacts from varying dissolved materials and particulate absorption [6]. Estimates of volume or mass concentration with transmissometers became popular when ocean-going instruments became commercially available [7,8]. SPM in the bottom boundary layers of natural waters vary by more than 3 orders of magnitude (from $<< 1$ to $> 1,000$ g m^{-3}). To maximize signal-to-noise ratios, the path-lengths of optical instruments are chosen based on the expected concentration (decreasing path-length as the expected concentration increases).

A multi-site comparison of the application of backscattering, side-scattering and attenuation as proxies of SPM demonstrated their ability to predict SPM within 36%, 51% and 54% respectively, for 95% of all cases [5]. The reasons for the difference is likely due to variable sensitivity of each property to particle size, packing and composition [1,9–11]. For example, the acceptance angle of transmissometers acts to filter out response from larger particles [12].

SPM has also been estimated from space-based measurements of radiance (e.g., [13]). In particular, remotely-sensed reflectance is most sensitive to the particulate backscattering coefficient in red and NIR wavelengths [14].

Size

Suspended sediments span in size from sub-μm-sized clay plates to mm-sized agglomerations of particles (flocs and aggregates) and sand. Terminology used to describe particles in suspension can be ambiguous. Here we refer to flocs as agglomerations of material that have relatively recently coagulated to form larger entities in suspension. The term aggregate refers to particles which consist of material that has undergone resuspension over several cycles during which they become more cohesive. While the component particles in flocs and aggregates may be similar, the density and settling velocity of aggregates is greater [15]. We ignore in this paper particles capable of sinking at speeds > 10 mm s^{-1}. These are rarely in suspension, and when they are in suspension, concentrations are so large that optical instruments typically saturate. In-situ optical proxies for size information include size distribution inverted from measurements of near forward scattering at several angles [16], the exponents of the power-law fit of the particulate attenuation spectrum or particulate backscattering spectrum [17–19] used to obtain a size tendency (or exponent of a power-law PSD if applicable), and fluctuation in optical signals to obtain the average size of suspended particles [20]. Images of particles have also been used to derive size distributions, particularly of larger flocs and aggregates (e.g., [1,3].

Theoretically, the maximal response of attenuation or scattering per volume (equivalent to mass if density is constant) occurs for single-grain sediment near $\frac{D}{\lambda}(n-1) \sim 1$ where λ is the wavelength in water ($= 0.75\lambda_{air}$), D is the particle diameter, and n is the index of refraction of the particle relative to water ([21], Fig. 1). For solid sedimentary particles with $n = 1.15$ at $\lambda_{air} = 660nm$, the maximal attenuation per mass occurs for small particles between 0.8-3.2 μm. This dependency decreases as $1/D$ as the diameter increases, and it increases for larges indexes of refraction (Fig. 1). Increases in

the index of refraction are typically associated with increases in the inorganic fraction in the particle suspension [22].

Composition

Composition of suspended particles spans from inorganic clays and silts of varied mineralogy to organic particles including both pigmented phytoplankton and non-algal particles. An optical proxy for composition (separating dominance by organic and inorganic particles) is the ratio of backscattering to total scattering [23,24]. Fluid-filled organic particles such as plankton have lower indexes of refraction compared to inorganic particles, resulting in a lower backscattering relative to total scattering. The ratio of chlorophyll containing particles to total particles, estimated from the ratio chlorophyll absorption to the particulate beam attenuation has also been used as a compositional proxy [25].

Suspended particles are often in flocs, which are fragile agglomerations of particles separated by relatively large volumes of interstitial fluid and transparent organic material [26]. These particles typically sink faster than their component particles [27,28]. They are broken as a result of turbulent shear, including that which is generated when they sink, limiting their maximal size to about 1cm [27,29]. In terms of their optical properties, flocs, if sufficiently porous, can maintain the efficiency of scattering of the particles of which they are made [30] and thus have higher magnitude mass-specific optical properties than a solid particle of the same size. Thus, for a floc with a solid fraction of 0.01 (99% water) the size of maximal beam-attenuation per volume (or mass) will be nearly 5 times larger than a solid particle made of the same material (Fig. 1). It follows that the flocculation state of a particle is critical to understand its optical properties (note that by our definition above aggregate have lower fluid fraction than flocs). These theoretical results were validated in a flocculation experiment that found that attenuation and backscattering to SPM ratios remained relatively constant despite large changes in particle size [31]. A proxy for packing has been derived from the ratio of beam attenuation (a mass concentration proxy) to the total particulate volume (obtained by inverting the forward scattering measurements with the LISST sensor [31–33]). Given that for a suspension of large particles the beam attenuation is a proportional of the total cross-section area (Babinet's principle) as well as found empirically to be a good proxy of mass, it follows that mass behaves like the cross-sectional area of the solid part of the particles comprising the floc (and that the floc fractal dimension is likely near a value of two). It follows that the above proxy should be proportional to the suspension's volume to cross-sectional area, or Sauter Diameter [33].

1.2. Particle dynamics

In this section we focus on the bottom boundary layer (for a recent review of the fluid dynamics of the BBL see [34]). The particle assembly C is a sum of many types of particles $C = \sum_i C_i$, each with their specific settling speed, composition, size and any other property that is relevant to either their hydrodynamic or their optical properties.

The general conservation equation for particles can be written as

$$\frac{\partial C_i}{\partial t} + \nabla(C_i \overrightarrow{u} + w_i) = \nabla(K\nabla C_i) + \Sigma_j f(C_{i-j}, C_j) + S_i \qquad (1)$$

where C_i is the mass concentration of particles of type i, t is time, $\overrightarrow{u}$ is the 3-D velocity field, w_i the settling velocity of these particles, K the diffusion coefficient, $f(C_{i-j}, C_j)$ represents aggregation and disaggregation dynamics creating and destroying C_i-type particles and S_i other sources and sinks (e.g. biological production/consumption of particles).

To solve Eq. (1) for a given flow field, one needs boundary conditions (e.g. flux or concentration of particles at the boundaries of the domain) and initial conditions (e.g. the state of the particles at time $t = 0$). Even then, Eq. (1) cannot be solved analytically except for very simple cases such as we will address next.

Eq. (1) is usually simplified to represent only the vertical dimension (z, which assumes that horizontal advection of horizontal gradients is negligible relative to vertical processes), and after time averaging (or assuming steady-state), results in:

$$w_i \frac{\partial C_i}{\partial z} = \frac{\partial K_{eddy} \partial C_i}{\partial z^2} + \Sigma_j f(C_{i-j}, C_j) + S_i \tag{2}$$

where C_i is here the time- (and horizontally-) averaged concentration of particles of type i, K_{eddy} is an eddy diffusion coefficient (representing the mixing by the small-scale turbulent field).

Large aggregation rates are associated with large particle concentrations, e.g. following a major resuspension event or during an algal bloom. Large disaggregation rates are associated with large fluid shears, e.g. in the wave boundary layer, which is a layer a few cm thick next to the bottom.

In the BBL, the law-of-the-wall is often invoked for which $K_{eddy} = \kappa u_* z$ where κ is a constant (~ 0.4 named after von Karman), u_* is the friction velocity (a function of BBL turbulence, e.g. due to wave and current shear). Neglecting aggregation dynamics, and integrating Eq.(2) in the vertical and solving the resulting ODE results in the Rouse equation:

$$C_i(z) = C_i(z_a) \left(\frac{z}{z_a} \right)^{-\frac{w_i}{\kappa u_*}} \tag{3}$$

where z_a is a reference depth where the particle concentration is known. It follows that particle concentration will decrease with height above the bottom. This is one of several different analytical solutions for the balance of settling and turbulent mixing (see review by [35]), all of which predict an increasing concentration towards the bottom for settling particles in the BBL.

1.3. Equation for the distribution of optical properties

Denoting a specific optical property by b_x, and the volume-specific optical property $\alpha_{v,i}$, then $b_x = \sum_i N_i V_i \times \alpha_{v,i}$, where N_i is the number concentration of particles of type-i and V_i each particle volume. $\alpha_{v,i}$ are typically computed using Mie code (which assumes homogeneous spherical particles) for solid particles and other models for flocs (e.g. [30]) requiring particle diameter, index of refraction (a function of composition), and wavelength of light as well as fractal dimension for flocs. The solutions are resonance-like functions of size (Fig. 1). Note that the application of Mie solution to backscattering has been challenged based on observations (e.g. [36]).

We can use Eq. (3) to obtain an equation for the optical property (neglecting aggregation and disaggregation dynamics and assuming constant density):

$$\sum_i w_i \alpha_{v,i} N_i V_i C_i = \frac{\partial K_{eddy} \partial b_x}{\partial z^2} \tag{4}$$

Equation 4 implies that only if we can assume a uniformity in settling velocity w_i, for example if the optical parameter used is sensitive to a very specific particle population (of settling speed w), can we expect:

$$b_x(z) = b_x(z_0) \left(\frac{z}{z_0} \right)^{-\frac{w}{\kappa u_*}}. \tag{5}$$

If Eq. (5) holds, then it can be used to infer the settling velocity of the particles most affecting the measured optical property. It follows that we expect the optical property to decrease away from the bottom (concentration of all settling particles should increase with depth). In addition, since the settling velocity of single grain particles increases with particle diameter (e.g. [37]), which is also true also for flocs [27,28], we expect size to increase towards the bottom. This, indeed, has been observed in BBLs. In particular [38], in a pioneering study, conducted a detailed analysis of the sediment size information that can be gleaned from optical and acoustical measurements in a BBL, using among other, fits of data to Rouse profiles (Eq. 5).

2. Examples from field data

Field data were obtained from a profiling instrument platform deployed at the Martha's Vineyard Coastal Observatory (MVCO) south of Martha's Vineyard, Massachusetts, at the 12m isobath in the summer of 2011, as part of the ONR-funded Optics and Acoustics and Stress In Situ (OASIS) experiment [39]. The platform was mounted on a pivoting arm that profiled every 20min from 10cm to 2m above bottom. The platform was equipped with variety of optical and acoustical sensors. Here we discuss data from a Sequoia LISST 100-X, a WETLabs EcoBB2f triptlet measuring backscattering at two wavelengths (532 and 650nm) and dissolved organic fluorescence, and a WETLabs AC-9 spectral absorption and beam attenuation meter. Water was pumped from an intake at the tip of the arm into the 10cm pathlength sampling volume of the AC-9. An automatic valve periodically routed the water sample through a 0.2um filter to remove particulates, leaving the dissolved fraction, to obtain calibration-independent particulate properties [40]. Shear velocity u_{*c} [cm/s] associated with mean flow in the bottom boundary layer (BBL) was inferred from a pair of acoustic Doppler velocimeter measurements (cf. [41]), and model estimates of the wave-current combined maximum shear velocity in the wave boundary layer (relevant to sediment resuspension) were determined using [42]. The location is dominated by the east-west semi-diurnal tidal currents, northward swell, and periodic storms (Fig. 2). The measurements discussed here were taken in the bottom boundary layer, which is mostly well mixed.

Waves and currents varied during the experiment, and we have selected four periods with distinctly different forcing and optical responses (Fig. 2). Two periods (Maria and Ophelia) were associated with offshore passage of hurricanes and arrival of swell waves at the study site. Another period (Spring tides) was associated with moderate wave conditions and strong spring tidal currents. The fourth period (Calm) was characterized by low waves and weaker neap tidal currents. For each of the four periods identified in Fig. 2, we show the distribution of the following optical properties (or properties inferred from optical measurements).

1. Beam attenuation $c_p(650)$ [m^{-1}] measured by the AC-9 and particulate backscattering coefficient ($b_{bp}(650)$ [m^{-1}] measured by the EcoBB2F provide proxies of particulate concentration (e.g. [5], where higher values associated with higher particle concentrations.
2. Exponent of the power-law fits of the particulate beam attenuation γ_{cp} [dimensionless] and backscattering γ_{bbp} [dimensionless] ($c_p = c_p(\lambda_0)(\lambda/\lambda_0)^{-\gamma_{cp}}$, with an analogous formula for γ_{bbp}) provide proxies for size distribution in the finer sizes (e.g. [17]). These exponents are proxies of size, with lower values associated with larger size averaged particles. γ_{cp} is biased towards the smaller (0.5 to 10µm) particles in the population [12], and γ_{bbp} may be more sensitive toward the larger particles [19].
3. Sauter diameter D_s [µm] is determined from the ratio of LISST measurements of volume and area concentrations, summed over size classes i as $D_s = 1.5 \sum V_i / \sum A_i$ and reciprocal of particle density $\rho_a^{-1} = \sum V_i / c_p$ [m ppm^{-1}], using the LISST-based c_p. Both are proxies for packing: larger values of D_s indicate larger, less-dense particle populations, and larger values of ρ_a^{-1} also indicate less-dense particle populations.
4. Particulate backscattering ratio $b_{bp}(532)/b_p(532)$ measured by the EcoBB2F ($b_{bp}(532)$) and by differencing of particlutale attenution and particulate aborption from the AC-9 ($b_p(532)$) was a proxy of composition. Increasing values of this ratio are associated with inorganic particles [23]. For very small particles, this ratio is also sensitive to size, increasing for smaller particles.
5. Chlorophyll to attenuation ratio $Chl/c_p(650)$ is another proxy of composition where higher values are associated with higher phytoplankton-based organic content [25].
6. LISST-based ratios of volume of fines to volume of micro-flocs (V_f/V_m) and volume of fines to volume of macro-flocs (V_f/V_M) helps elucidate floc dynamics. We use 20µm as the boundary between fines and micro-flocs and 140µm as the boundary between micro- and macro-flocs, and neglect the first and last three bins of the LISST volumes. These ratios are proxies for composition, where higher values indicate larger proportions of smaller particles.

We selected one-hour intervals during each of the different periods identified in Fig. 2 when the concentration profiles estimated from attenuation decreased monotonically with elevation above the seabed, and were relatively well approximated by a linear profile in log-log coordinates (Eq. 5). These profiles were consistent with the steady-state Rouse balance discussed above, suggesting that we might be able to neglect the effects of horizontal gradients and temporal transients. The data represent the average of three consecutive profiles, each of which took 20min to complete. All properties are displayed as function of elevation above the bottom in Fig. 3-6. Trends in vertical profiles and representative values (mean and standard deviation) for each time period are summarized in Tab. 1 and 2.

2.1. SPM

The overall concentration of SPM fluctuated through the experiment (Fig. 2), as indicated by variations $c_p(650)$ and $b_{bp}(650)$. The time series of $c_p(650)$ at 1m above the bottom indicates increased SPM during Maria and Ophelia, somewhat reduced SPM during the Spring tides, and low SPM during the Calm period. Mean values of $c_p(650)$ in the 60-min profiles ranged from about 1 m^{-1} during the Calm period to 12 m^{-1} during Ophelia, when wave-induced resuspension increased SPM in the BBL. Mean values of $b_{bp}(650)$ generally covaried with to $c_p(650)$, ranging from 0.02 m^{-1} to 0.30 m^{-1} for the same periods. The profiles of $c_p(650)$ and $b_{bp}(650)$ invariably decreased with elevation, and the ones examined here were nearly log-linear (Rouse-like). However, there was typically more scatter in the profiles of $b_{bp}(650)$, as evidenced by their lower r^2 (Tab. 2), especially during periods of lower concentrations.

2.2. Settling velocities assuming Rouse profiles

Mean apparent settling velocities inferred from c_p and b_{bp} profiles ranged from about 0.1 to 4 cm/s. Although the settling velocities estimated were similar, and showed similar trends over the four periods, $w_{s,cp}$ was usually faster than $w_{s,bbp}$. c_p is less sensitive to large, low-density particles, so settling-velocity estimates from c_p were likely to favor smaller, denser, faster-settling aggregates and single-grained particles. Inferred settling speeds were fastest when D_s was smallest (Maria and Ophelia), which means that particle density, rather than size, determined the inferred settling speeds. This suggests that the flocs with larger D_s observed by the LISST were porous and fragile. The faster settling velocities obtained during energetic periods occurred when the ratio of single grains to macro-flocs was highest, meaning that large flocs were relatively scarce. The simplest explanaions for these observations are that large fragile flocs were disrupted by turbulence and/or that smaller denser particles were resuspended from the bed. These relatively simple particle dynamics are not consistent with the higher-than-expected observed settling velocities inferred from the Rouse profiles during strong forcing (Maria and Ophelia). The bottom sediment at MVCO is well-sorted fine sand with a median diameter of 150 μm [39,43]. The inferred settling velocities during Maria (1 cm/s) and Ophelia (4 cm/s) correspond to sand grains of 140 μm and 320 μm, respectively [44]. If grains this large were resuspended during energetic events and were therefore responsible for the relatively steeply declining concentration profiles above the bed, then their presence would have been reflected in D_s that were larger than the observed values. One possible reason that we are inferring such large velocities is that flocs scavenged small particles at the top of the profiles, sank, and were disrupted at the bottom of the profile, thereby injecting small particles into suspension near the bed. This mechanism is consistent with observed increases in D_s away from bottom in both Fig. 4 and 5, resulting in steeper c_p and b_{bp}. During the calm period, settling velocities based on the Rouse profile are a mm/sec, consistent with typcial floc settling velocities ([27,45]).

2.3. Size

Size was often correlated across the different proxies but with significant departure at specific times, highlighting the different particles to which each optical proxy is sensitive. While γ_{cp} and γ_{bbp}

often had similar depth distributions, their values differed: γ_{bbp} was always significantly smaller. In one case the values had opposite trends with depth. The change in value and higher variability in γ_{bbp} may be due to the effect of absorption, which could depress scattering more at wavelengths where particulate absorption is higher, typically in the green. Lower values of γ_{bbp} may also have been due to the fact that b_{bp} is more sensitive to large particles than is the beam attenuation of the ac-9. The reversal in trend occurred when the suspension was enriched with macro-flocs compared to micro-flocs away from the bed with opposite trends in V_f/V_m and V_f/V_M (Fig. 4).

Sauter diameter and the reciprocal of floc density were well correlated, suggesting they provide similar information. Beam attenuation is a robust proxy for mass because both mass and attenuation correlate with cross-sectional area for typical flocculated particle suspensions. As a result volume over area (i.e. Sauter diameter) is proportional to volume over mass (i.e., inverse density). Density was high (displayed ρ_a^{-1} being low) when forcing was large (Fig. 3 and 5), due to resuspension and to floc breakup, and when conditions were calm, because of deposition of, lower-density, faster-sinking large flocs. During the spring tides, when large flocs were relatively more abundant, density was lowest.

Particle size increased away from the bed during spring tides. This observation does not fit neatly with Rouse dynamics. The depth-distribution of size may be due to either resuspension of large single grains and aggregates or breakup of flocs near the bed where turbulence is more intense and reformation of flocs away from the bed where turbulence is weaker. Both mechanisms could increase the Rouse-based settling velocity, the former by introducing a source of fast-sinking particles from the bed and the latter by providing a source of fines from floc breakup to the nearbed region.

2.4. Composition

The backscattering ratio was relatively high (>0.02) during the full deployment suggesting domination by inorganic particles. Curiously, the ratio was smaller during the energetic events than it was during the spring tides, suggesting that resuspension caused by longer-period waves from Ophelia and Maria excavated densely packed organic material that was stored in the interstices of the bed sediment at the site. Alternatively, more organic-rich material may have been advected into the site by these events. The backscatter ratio was not correlated to the Chl_a/c_p ratio, which always increased away from the bed, consistent with chlorophyll-containing particles being at lower concentration relative to other particles closer to the bed. This observation supports resuspension of degraded, non-chlorphyllous organic material from the bed, possibly in the form of aggregates, as an explanation for lower backscatter ratios during energetic events. Chl_a profiles usually showed no trend with elevation (not shown), consistent with the hypothesis that the increase Chl_a/c_p ratio away from bed was due to enrichment in faster settling non-algal particles near the bottom.
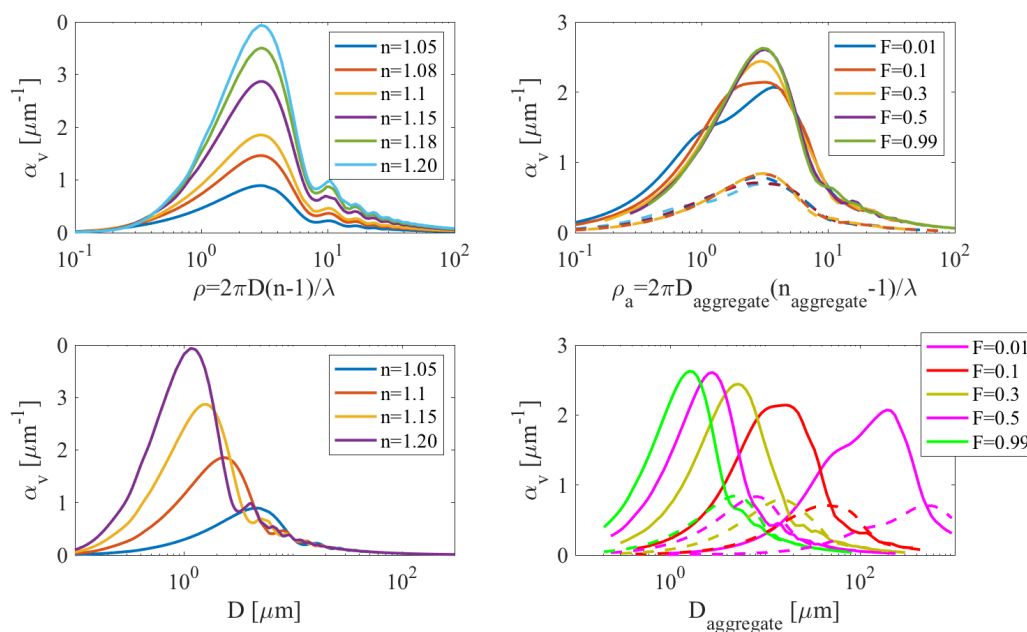
2.5. Figures, Tables and Schemes

Figure 1. Top panels: Volume specific beam-attenuation (α_v for solid particles (left) and aggregates (right) as function of $\frac{2\pi D}{\lambda_{water}}(n-1)$ where D is diameter, λ_{water} the wavelength in water and n the index of refraction (which increases between organic and inorganic particles). For aggregates $n_{aggregate} = 1 + F(n-1)$ where F is the solid fraction and n the index of refraction of the particles the aggregate is comprised of. In all cases, the volume used to compute α_v is that of the solid fraction. Bottom panels: same as on top but plotted as function of particle diameter. In all the computations $\lambda_{air} = 660nm$ and $n' = 0.0001$, where n' is the imaginary part of the index of refraction, representing absorption.
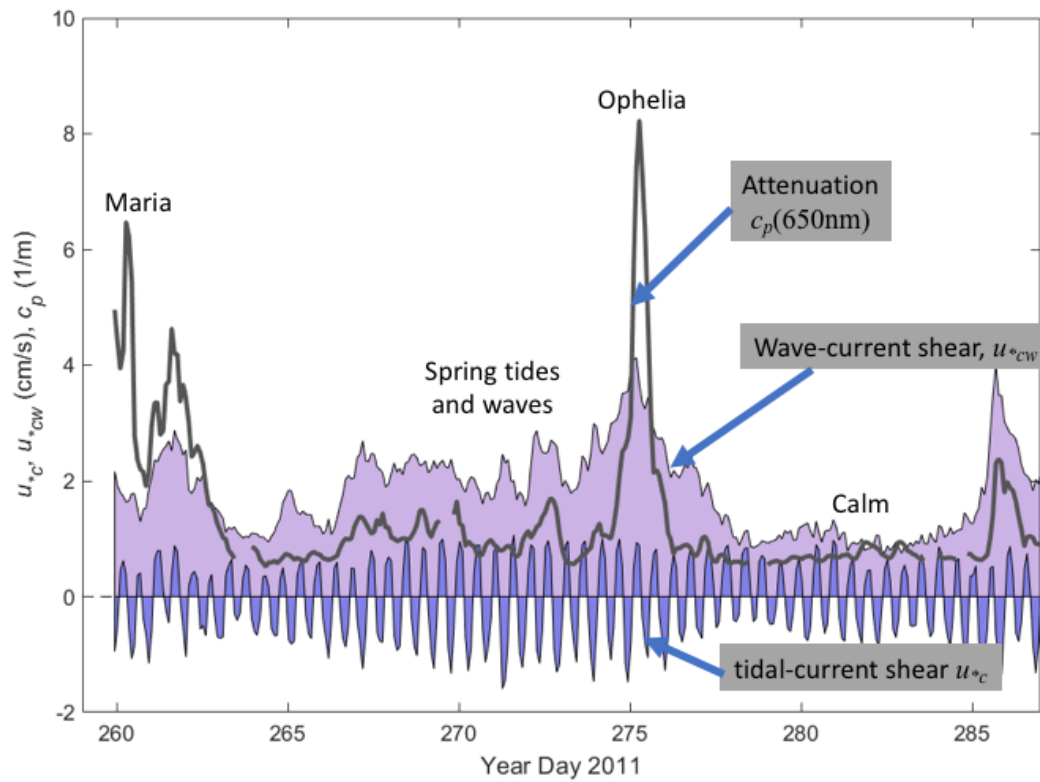
Figure 2. Time series of conditions at the 12-m MVCO site during the OASIS deployment in 2011: beam attenuation at 650nm measured at 1m above the bottom (gray), tidal current shear velocity u_{*c} (blue) and combined wave-current shear velocity u_{*cw} (purple) . Notice labels describing specific periods.
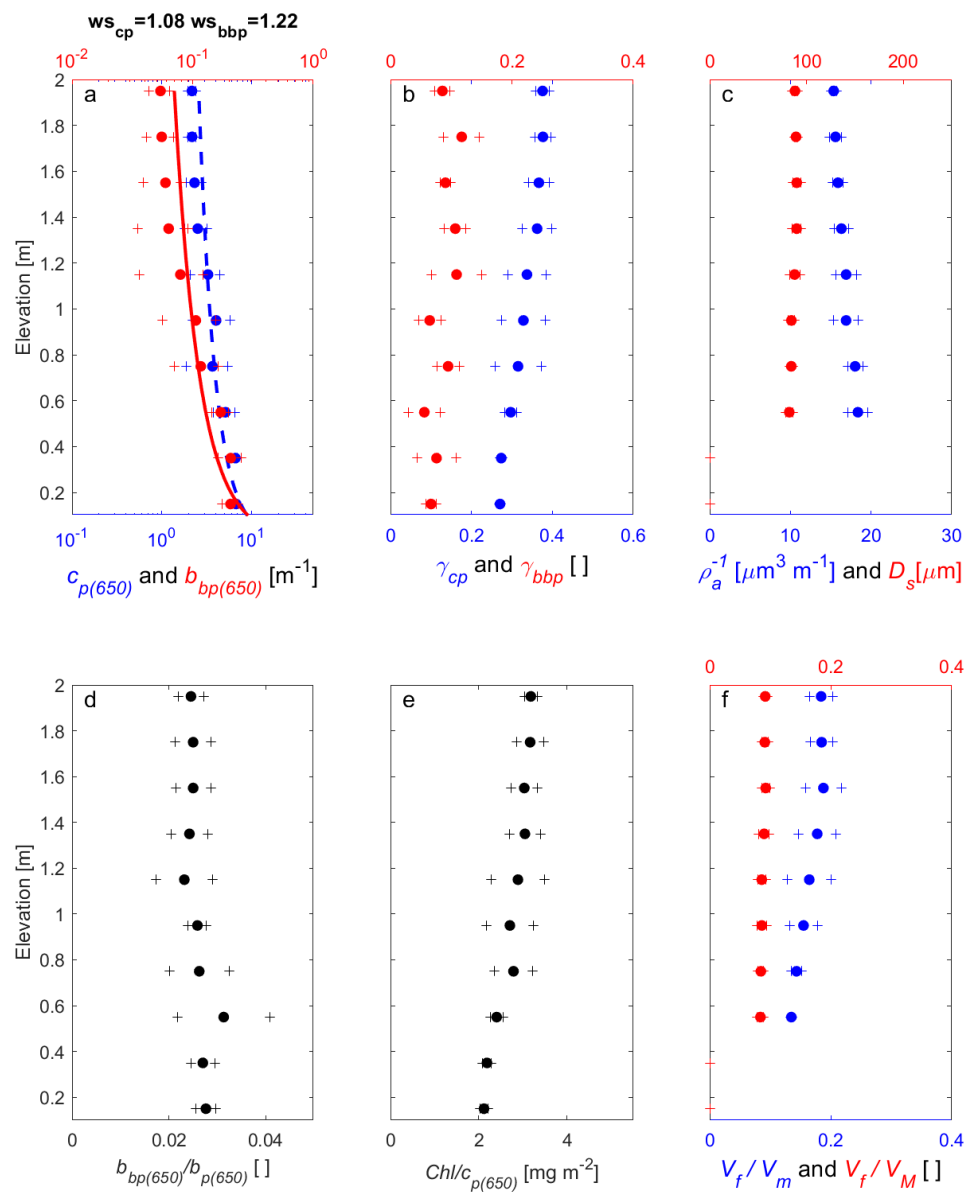
Figure 3. Profiles of optical parameters at MVCO on day 261.1 when waves from Hurricane Maria were coming to shore (see Fig. 2). a) Beam attenuation ($c_p(650)$, blue) and particulate backscattering ($b_{bp}(650)$, red), b) power-law exponent of $c_p(650)$ (blue) and $b_{bp}(650)$ (red), c) Sauter Diameter (red) and inverse particle density (blue), d) backscattering ratio (black), e) chlorophyll divided by $c_p(650)$, and e) volume ratios: fine to micro-flocs (blue) and fine to macro-floc (red). Standard deviation about the mean values for three consecutive profiles (60 minutes) are shown with crosses. Dashed lines in panel (a) are log-log fits to the data, from which the settling velocities shown on the top of the panel were computed.
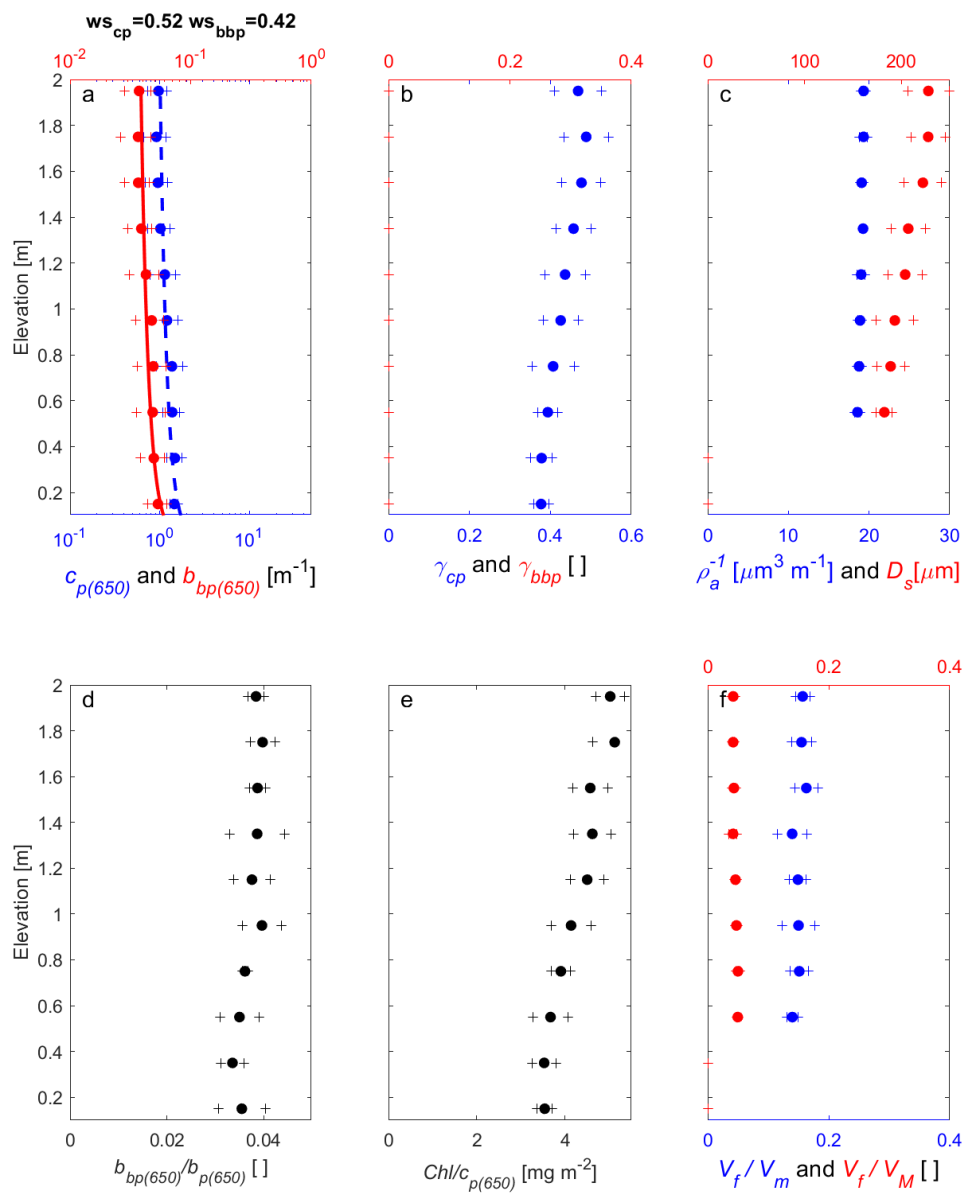
Figure 4. Profiles of optical parameters at MVCO on day 268.62 during Spring tides and moderate waves. Panels are as described in Fig. 3).
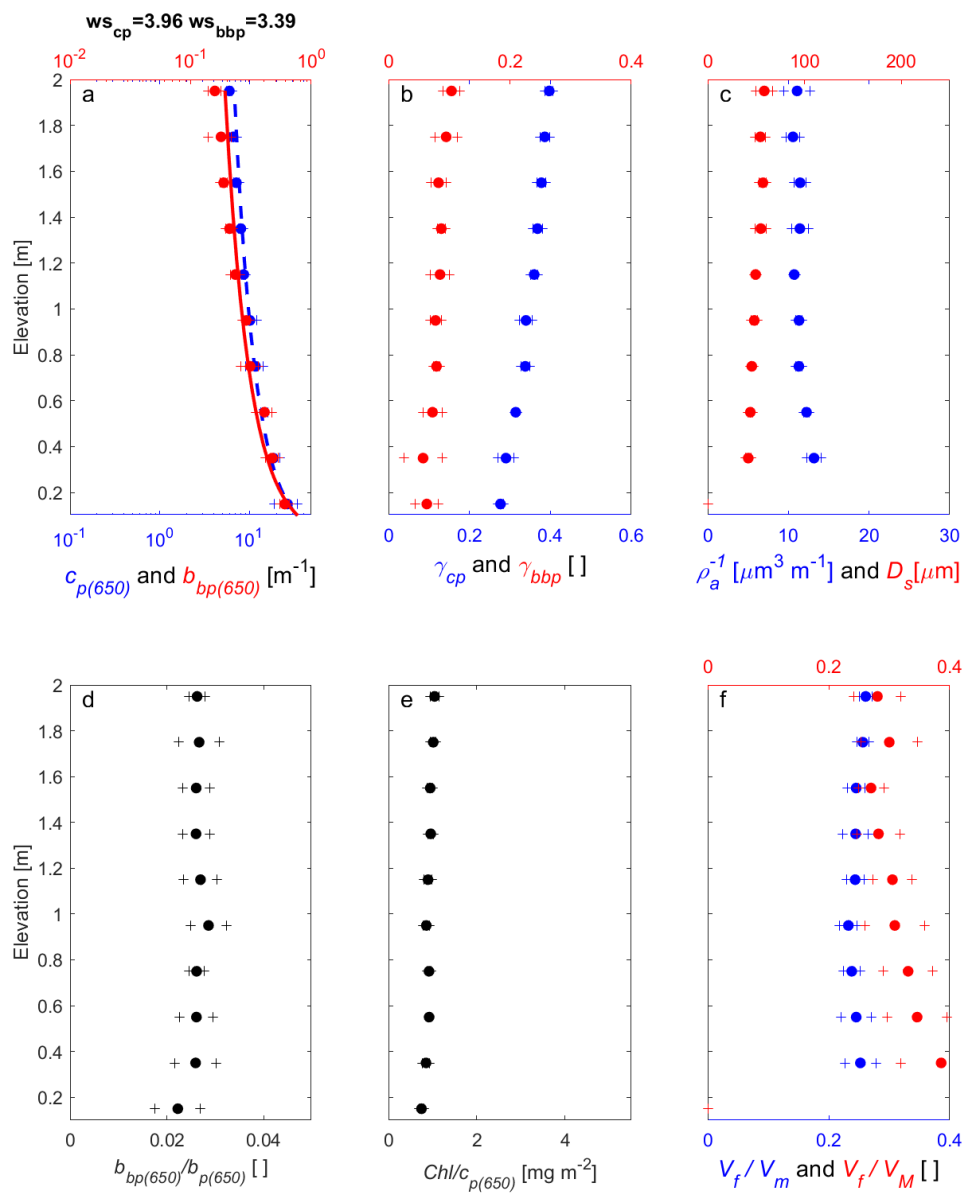
Figure 5. Profiles of optical parameters at MVCO on day 275.20 during the passage of Hurricane Ophelia. Panels are as described in Fig. 3).
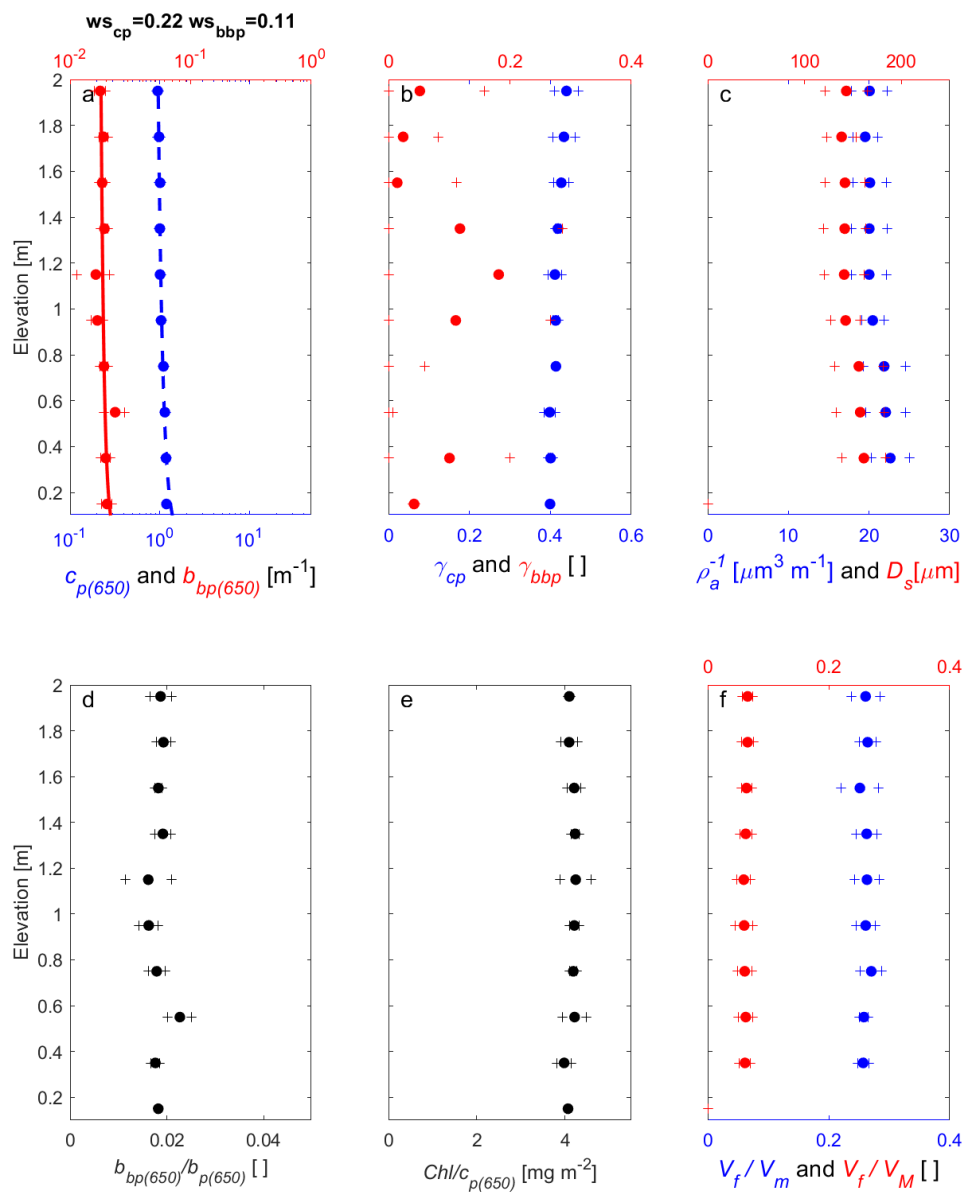
Figure 6. Profiles of optical parameters at MVCO on day 281.93 during Spring tides and moderate waves. Panels are as described in Fig. 3).

Table 1. Trends in particle parameters as function of depth based on the average of three profiles in the BBL in each of the four periods denoted in Fig. 2. $\searrow$ and $\nearrow$ denote profiles that are decreasing or increasing (respectively) with elevation above the bottom, $\sim$ denotes that the trend is weak, and $|$ denotes that there is no trend with elevation.

parameter	Maria	Spring tide	Ophelia	Calm
$b_{bp}(650)$	$|$	$\searrow$	$\searrow$	$\sim\searrow$
$c_p(650)$	$\searrow$	$\searrow$	$\searrow$	$\searrow$
γ_{bbp}	$\nearrow$	$\searrow$	$\nearrow$	$\sim\nearrow$
γ_{cp}	$\nearrow$	$\nearrow$	$\nearrow$	$|$
D_s	$|$	$\nearrow$	$\sim\nearrow$	$\sim\searrow$
ρ_a^{-1}	$\sim\searrow$	$\nearrow$	$\sim\nearrow$	$\sim\searrow$
$b_{bbp}/b_p(650)$	$\sim\nearrow$	$\nearrow$	$|$	$|$
$Chl/c_p(650)$	$\nearrow$	$\nearrow$	$\sim\nearrow$	$\nearrow$
V_f/V_m	$\nearrow$	$\sim\nearrow$	$\sim\nearrow$	$\sim\searrow$
V_f/V_M	$\nearrow$	$\searrow$	$|$	$\sim\nearrow$

Table 2. Mean and standard-deviation (in brackets) optical particle parameters computed based on the average of three profiles in the BBL in each of the four periods denoted in Fig. 2. The wave-current and current shear velocities and the settling velocities inferred from fitting the Rouse profile to c_p and b_{bp} are also listed, with regression coefficient r^2 in brackets.

parameter	Maria	Spring tide	Ophelia	Calm
$b_{bp}(650)$ $[m^{-1}]$	0.11(0.06)	0.04(0.01)	**0.30**(0.14)	0.02(0.002)
$c_p(650)$ $[m^{-1}]$	3.87(1.77)	1.19(0.22)	**11.81**(6.51)	1.06(0.09)
γ_{bbp}	**0.09(0.02)**	-0.14(0.06)	0.0(0.01)	0.06(0.07)
γ_{cp}	0.33(0.04)	**0.43(0.04)**	0.34(0.04)	0.42(0.01)
D_s $[\mu m]$	87.3(3.0)	**210.7**(20.5)	50.4(6.0)	147.0(8.7)
ρ_a^{-1} $[m\,\mathrm{ppm}^{-1}]$	16.6(1.1)	19.1(0.3)	11.5(0.8)	**20.8(1.1)**
$b_{bp}(650)/b_p(650)$	0.03(0.002)	**0.04**(0.002)	0.03(0.002)	0.02(0.002)
$Chl/c_p(650)$ $[\mu g m^{-2}]$	2.8(0.4)	**4.3**(0.6)	0.9(0.1)	4.2(0.1)
V_f/V_m	0.17(0.02)	0.15(0.01)	0.25(0.01)	**0.26**(0.01)
V_f/V_M	0.09(0.004)	0.04(0.002)	**0.31**(0.04)	0.06(0.002)
u_{*wc} [cm/s]	2.3	2.4	**4.1**	0.8
u_{*c} [cm/s]	0.6	0.7	**1.8**	0.4
ws_{bbp} [cm/s]	1.22(0.72)	0.42(0.72)	**3.39(0.94)**	0.11(0.00)
ws_{cp} [cm/s]	1.08(0.80)	0.52(0.66)	**3.96(0.99)**	0.22(0.95)

3. Discussion

Optical properties are useful for constraining particulate properties in BBLs and often behave in ways consistent with our understanding of their dynamics. The BBL is a dynamic region where particles segregate based on their settling velocity and their aggregation/disaggregation dynamics, making it necessary to use measurements that respond differently to their properties to elucidate this segregation.

While in all of the the cases illustrated here a settling velocity based on the Rouse balance could be assigned and varied by an order of magnitude between profiles, it is clear that the flocs, the dynamics of which were neglected in the Rouse equation, varied in the water column. Breakup and aggregation in the case of spring tides in particular likely affected significantly the profiles of observed optical properties. In all cases the values of the inferred settling velocities were significantly larger than peer settling velocities of particles expected to dominate the attenuation and backscattering, requiring measurements of the larger fraction to understand the distribution of optical properties in BBLs.

4. Conclusions

[38] stated in the conclusion of their paper that "We are approaching the point where we can begin to measure sediment transport on a size class by size class basis". This prediction has not taken place, in particular, we believe, because these measurements could not yet be used to constrain sediment-transport models, except when highly simplifying assumptions, such as Rouse dynamics were assumed.

As we show here each optical measurement can provide a snapshot of the distribution of a size/composition/packing-weighted segment of the particulate population. Combinations of optical measurements provides information about bulk intensive properties (concentration, size, composition and packing) of the particulate assembly, as well as the possibility to differentiate size fractions. The co-location of these independent/biased measurements clearly provides more information than could be available from each measurement on its own.

It is also clear from the field data that aggregation dynamics cannot be neglected when interpreting profiles of properties most sensitive to the small particles (e.g. beam attenuation) as the flocs are both a sink and source for fine particles. Hence the settling velocity inferred from fitting a power-law profile should be interpreted qualitatively and not quantitatively as the true settling speed of the suspension (e.g. to compute clearance rates).

Addition of acoustical measurements [38] could further constrain the particle dynamics and distribution as they are sensitive differently to composition, size and packing than optical properties. For example, for acoustic backscattering at the MHz range, aggregation decreases the signal [46] while being sensitive to large single grain particles (while optical attenuation is not).

Advances in models that now include resuspension as well as aggregation/disaggregation dynamics (e.g. [47]) that can be coupled with optical models (for single grains as well as flocs) now makes it possible to compare predicted optical properties with in-situ measurements, opening the possibility to assimilate such data in the future. In order to assimilate such properties to constrain or compare to output of dynamic sediment models, the model variables (concentrations of different types of particles) need to be expressed in terms of optical properties, requiring optical models to translate between bio-geochemical and optical properties. Such models could be based on bulk empirical relationships and/or on highly detailed theoretical models (which have idealized assumptions). It is critical that such models be developed to improve dynamical models of sediment dynamics.

Author Contributions: P.H., T.M., E.B., and C.S. conceived, designed, and performed the experiments. C.S. and E.B. processed the data; E.B. conceived the paper and wrote the first draft; C.S., P.H. and T. M. contributed to the writing.

Abbreviations

The following abbreviations are used in this manuscript:

BBL: bottom boundary layer
MVCO: Martha's Vineyard Coastal Observatory
OASIS: Optics and Acoustics and Stress In Situ

ONR: Office of Naval Research
SPM: suspended particulate mass
USGS: U.S. Geological Survey
WHOI: Woods Hole Oceanographic Institution

References

1. Hill, P. S.; Boss; E.; Newgard, J.P.; Law, B. A.; Milligan, T. G. Observations of the sensitivity of beam attenuation to particle size in a coastal bottom boundary layer.*J. Geophys. Res.* **2011**, *116*, C02023, doi:10.1029/2010JC006539.

2. Downing, J. Twenty-five years with OBS sensors: The good, the bad, and the ugly. *Cont. Shelf Res.* **2006**, *26*, 2299-2318.

3. Mikkelsen, O. A. ; Hill P. S. ; Milligan, T. G.; Chant, R. G. In situ particle size distributions and volume concentrations from a LISST100 laser particle sizer and a digital floc camera. *Cont. Shelf Res.* **2005**, *25*, C02023, 1959–1978.

4. ACT [Alliance for Coastal Technologies]. Measuring turbidity in coastal waters. ACT WR05-08, UMCES/CBL 06-026.**2005**

5. Boss, E.; Taylor, L.; Gilbert S.;Gundersen, K.; Hawley, N.; Janzen, C.; Johengen, T.; Purcell, H.;Robertson, C.;Schar, D. W.; Smith, G. J.; Tamburri, M. N. Comparison of inherent optical properties as a surrogate for particulate matter concentration in coastal waters. *Limnnol. Ocean. Meth.*, **2009**, *7*, 803-810.

6. Stramski, D; Babin, M. ; Wozniak, S. Variations in the optical properties of terrigenous mineral-rich particulate matter suspended in seawater. *Limnol. Oceanogr.*, **2007**, *52*, 2418–2433.

7. Petzold, T. J.; Austin, R. W. An Underwater Transmissometer For Ocean Survey Work. In *Underwater Photo-Optical Instrumentation Applications II*; International Society for Optics and Photonics, **1968**, *12*, pp. 133–141.

8. Bartz, R.; Ronald, J.; Zaneveld, V.; Pak, H. A Transmissometer For Profiling And Moored Observations In Water. In *Ocean Optics V*; International Society for Optics and Photonics, **1978**, *160*, pp. 102–110.

9. Stemmann, L.; Boss, E. Plankton and particle size and packaging: From determining optical properties to driving the biological pump. *Annu. Rev. Mar. Sci.* , **2012**, *4*, 263-290.

10. Stramski, D.; Boss, E.; Bogucki, D.; Voss, K. J.. The role of seawater constituents in light backscattering in the ocean. *Prog. Ocean.* , **2004**, *61*, 27-55.

11. Hill, P. S.; Bowers, D. G.; Braithwaite, K. M. The effect of suspended particle composition on particle area-to-mass ratios in coastal waters. *Methods in Oceanography*, **2013**, *7*, 95-109.

12. Boss, E.; Slade W. H.; Behrenfeld, M.; Dall'Olmo, G. Acceptance angle effects on the beam attenuation in the ocean. *Opt. Exp.*, **2009**, *17(3)*, 1535-1550.

13. Stumpf, R. P. Sediment Transport in Chesapeake Bay during Floods: Analysis Using Satellite and Surface Observations. *J. Coast. Res.*, **1988**, *4*, 1–15.

14. Nechad, B.; Ruddick K. G.; Park, Y. Calibration and validation of a generic multisensor algorithm for mapping of total suspended matter in turbid waters.*Remote. Sens. Envir.*, **2010**, *114*, 854-866.

15. Lavallee, K. D.; Kineke, G. C.; Milligan, T.G. Variability of cohesive particle characteristics in an energetic estuary. Estuaries and Coasts.

16. Agrawal, Y.; Pottsmith, H. Instruments for particle size and settling velocity observations in sediment transport. *Mar. Geol.* **2000**, *168*, 89–114.

17. Slade, W. H.; Boss, E. Spectral attenuation and backscattering as indicators of average particle size. *Appl. Opt.*, **2015**, *54*, 7264-7277.

18. Boss, E. ; Twardowski, M. S.; Herring, S. Shape of the particulate beam attenuation spectrum and its relation to the size distribution of oceanic particles. *Appl. Opt.*, **2001**, *40*, 4885-4893.

19. Tao, J.; Hill, P. S.; Boss, E. S.; Milligan, T. G. Variability of suspended particle properties using optical measurements within the Columbia River Estuary. *J. Geophys. Res.: Oceans*, **2018**, *123*, https://doi.org/10.1029/2018JC014093

20.   Briggs, N. T.; Slade W. H. ; Boss, E. ;Perry, M. J. Method for estimating mean particle size from high-frequency fluctuations in beam attenuation or scattering measurements. *Appl. Opt.* **2013**, *52*, 6710-6725.

21.   van de Hulst, H. C. *Light Scattering by Small Particles*; John Wiley and Sons, 1957; reprint, Dover, 1981;

22.   Carder, K. L.; Betzer, P. R.; Eggimann D. W. Physical, chemical and optical measures of suspended-particle concentrations: Their intercomparison and application to the West African Shelf. In *Suspended solids in Water*; Gibbs, J., Ed.; Plenum: New York, USA, 1974; pp. 173-193.

23.   Twardowski M.; Boss E.; MacDonald, J. B.; Pegau, W. S.;Barnard, A. H.; Zaneveld, J. R. V. A model for estimating bulk refractive index from the optical backscattering ratio and the implications for understanding particle composition in case I and case II waters. *J. Geophys. Res.* **2001**, *106*, 129–142.

24.   Loisel, H.; Meriaux, X. ; Berthon, J.-F.; Poteau Antoine. Investigation of the optical backscattering to scattering ratio of marine particles in relation to their biogeochemical composition in the eastern English Channel and southern North Sea. *Limnol. Oceanogr.*, **2007**, *52*, 739-752.

25.   Boss, E.; Pegau, W. S.; Lee, M.; Twardowski, M.; Shybanov, E.; Korotaev, G.; Baratange, F. (Particulate backscattering ratio at LEO 15 and its use to study particle composition and distribution. *J. Geophys. Res.*, **2004**, *109*, doi: 10.1029/2002JC001514.

26.   Li, X.; Passow, U.; Logan, B. E. Fractal dimensions of small (15-200 *μm*) particles in Eastern Pacific coastal waters. *Deep Sea Res. Part I*, **1998**, *45(1)*, 115–131.

27.   Hill, P. S.; Syvitiski, J. P.; Cowan, E. A.; Powell, R. D. In situ observations of floc settling velocities in Glacier Bay, Alaska. *Mar. Geol.*, **1998**, *145(1-2)*, 85-94.

28.   Johnson, C.; Li, X.; Logan B. Settling Velocities of Fractal Aggregates. *Environ. Sci. Technol.*, **1996**, *30*, 1911-1918.

29.   Hill, P. S.; Voulgaris, G.; Trowbridge, J. H. Controls on floc size in a continental shelf bottom boundary layer.*J. Geophys. Res.*, **2001**, *106*, 9543-9549.

30.   Boss, E.; Slade, W.H.; Hill, P. Effect of particulate aggregation in aquatic environments on the beam attenuation and its utility as a proxy for particulate mass. *Opt. Exp.* **2009**, *17*, 9408-9420.

31.   Slade, W. H.; Boss, E.; Russo, C. Effects of particle aggregation and disaggregation on their inherent optical properties. *Opt. Exp.* **2011**, *19*, 7945-7959.

32.   Neukermans, G.; Loisel, H.; Meriaux, X.; Astoreca, R.; McKee, D.; In situ variability of mass-specific beam attenuation and backscattering of marine particles with respect to particle size, density, and composition. *Limnol. Oceanog.*, **2012**, *57*, 124-144.

33.   Hurley, A. J.;Hill, P. S.; Milligan, T. G.; Law, B. A. Optical methods for estimating apparent density of sediment in suspension. *Meth. Oceanog.*, **2016**, *17*, 153-168.

34.   Trowbridge, J. H.; Lentz, S. J. The bottom boundary layer. *Ann. Rev. Mar. Sci.*, **2018**, 397-420.

35.   Toorman, E. A. Sediment-laden turbulent flow: a review of theories and models. *Report HYD/ET/00/COSINUS1, Hydraulics Laboratory, K. U. Leuven*, **2000**.

36.   Dall'Olmo, G.; Westberry, T.K.; Behrenfeld, M.J.; Boss, E.;Slade, W. H.Significant contribution of large particles to optical backscattering in the open ocean. *Biogeosciences*, **2009**, *6*, 947-967.

37.   Dietrich, W. E. Settling velocity of natural particles. *Water Resources Res.*, **1982**, *18(6)*, 1615–1626.

38.   Lynch, J. F.; Irish, J. D.; Sherwood, C. R.; Agrawal, Y. C. Determining suspended sediment particle size information from acoustical and optical backscatter measurements. *cont. Shelf Res.*, **1994**, *14*, 1139-1165.

39.   Sherwood, C.R.; Dickhudt, P.J.; Martini, M.A.; Montgomery, E.T.; Boss, E.S. Profile measurements and data From the 2011 Optics, Acoustics, and Stress In Situ (OASIS) project at the Martha's Vineyard Coastal Observatory. U.S. Geological Survey Open-File Report 2012-1178, **2012**, http://pubs.usgs.gov/of/2012/1178/.

40.   Slade, W.H; Boss, E.; Dall'Olmo, G.; Langner, M.R.; Loftin, J.; Behrenfeld, M.J.; Roesler, C.; Westberry, T. K. Underway and moored methods for improving accuray in measurement of spectral particulate absorption and attenuation. *J. Atmos. Ocean. Tech.*, **2010**, *27*, 1733-1746.

41.   Trowbridge, J. H. On a Technique for Measurement of Turbulent Shear Stress in the Presence of Surface Waves. *J. Atmos. Oceanic Technol.*, **1998**, *15*, 290–298.

42.   Madsen, O. S. , Spectral wave-current bottom boundary layer flows. *Coastal Engineering 1994. Proceedings, 24th International Conference Coastal Engineering Research Council*, ASCE, Kobe, **1994**, 384-398.

43.   Goff, J. A.; Mayer, L. A.; Traykovski, P.; Buynevich, I.; Wilkens, R.; Raymond, R.; Glang, G.; Evans, R. L.; Olson, H.; Jenkins, C. Detailed investigation of sorted bedforms, or "rippled scour depressions," within the Martha's Vineyard Coastal Observatory, Massachusetts. *Cont. Shelf Res.*, **2005**, *25*, 461–484, doi:10.1016/j.csr.2004.09.019.

44.   Soulsby, R. Dynamics of Marine Sands. Thomas Telford: London, 1997; 215 pp.

45.   Curran K. J.; Hill, P. S.; Milligan, T. G.; Mikkelsen, O. A.; Law, B. A.; Durrieu de Madron, X.; Bourrin, F.; Settling velocity, effective density, and mass composition of suspended sediment in a coastal bottom boundary layer, Gulf of Lions, France. *Cont. Shelf Res.*, **2007** *27*, 1408–1421.

46.   Russo, C. An acoustical approach to the study of marine particles dynamics near the bottom boundary layer. PhD dissertation, University of Maine, Orono, ME, USA; 2011;

47.   Sherwood, C. R.; Aretxabaleta, A. L.; Harris, C. K.; Rinehimer, J. P.; Verney, R.; Ferré, B. Cohesive and mixed sediment in the Regional Ocean Modeling System (ROMS v3.6) implemented in the Coupled Ocean–Atmosphere–Wave–Sediment Transport Modeling System (COAWST r1234). *Geosci. Model Dev.*, **2018**, *11*, 1849–1871.